Electronic Supplementary Material (ESI) for Dalton Transactions.

Structural Dynamics of a Thermally Silent Fe^{II} Spin Crossover Defect-Grid Complex

Jose de Jesus Velazquez-Garcia[a]*, Krishnayan Basuroy[a], Darina Storozhuk[a], Joanne Wong[b], Serhiy Demeshko[b], Franc Meyer[b], Robert Henning[c] and Simone Techert[ad]

[a]Photon Science - Structural Dynamics in Chemical Systems, Deutsches Elektronen-Synchrotron DESY, Notkestraße 85, Hamburg, 22607, Germany

[b]Institut für Anorganische Chemie, Georg-August-Universität Göttingen, Tammannstraße 4, Göttingen, 37077, Germany

[c]Center for Advanced Radiation Sources, The University of Chicago, Argonne National Laboratory, 9700 South Cass Ave, Lemont, Illinois, 90439, USA

[d]Institut für Röntgenphysik, Georg-August-Universität Göttingen, Friedrich-Hund-Platz 1, Göttingen, 37077, Germany

Characterization

Table S1. Crystal data and structure-refinement parameters of **FE3** at 100K.

Temperature	100K
Empirical Formula	C100 H74 B4 F16 Fe3 N28
Crystal colour/habit	Black/block
Crystal size (mm)	(0.090x0.050x0.030)
Crystallizing solvent	Acetonitrile
Crystal system/ Space group	Triclinic/ P-1
a (Å)	14.010 (3)
b (Å)	14.480 (3)
c (Å)	24.320 (5)
α (°)	91.520 (3)
β (°)	95.920 (3)
γ (°)	107.67 (3)
Volume ($Å^3$)	4467.1 (18)
Z/Z'	2/1
Molecular Weight	2182.66
Calculated density (g/cm3)	1.553
F(000)	2224.0
Radiation	Synchrotron (λ=0. 61990 Å)
θ range (°)	1.290/22.648
Scan type	φ
Measured reflections	62278
Unique reflections	16815
Observed reflections [|F|> 4σ(F)]	16189
Final R (%)	5.31
wR2 (%)	14.84
Good-of-fit on F^2(S)	1.049
Δρ max (e. $Å^{-3}$)	2.05
Δρ min (e. $Å^{-3}$)	-0.94
No of restrains/parameters	208/1483
Data [|F|> 4σ(F)]-to-parameter ratio	10.92:1

Table S2. Selected bond lengths and bond angles for compound **FE3** at 100K.

Bond lengths (Å)		Bond angles (°)			
Fe(A)-N1	1.979 (2)	N8-Fe(A)-N7	79.84 (8)	N21-Fe(B)-N16	96.55 (9)
Fe(A)-N2	1.908 (2)	N8-Fe(A)-N1	98.53 (9)	N21-Fe(B)-N18	88.06 (9)
Fe(A)-N3	1.973 (2)	N8-Fe(A)-N2	174.26 (8)	N21-Fe(B)-N19	160.73 (10)
Fe(A)-N7	2.003 (2)	N8-Fe(A)-N3	101.05 (9)	N20-Fe(B)-N16	105.16 (10)
Fe(A)-N8	1.907 (2)	N8-Fe(A)-N9	79.95 (8)	N20-Fe(B)-N18	94.64 (10)
Fe(A)-N9	2.026 (2)	N7-Fe(A)-N9	159.78 (8)	N20-Fe(B)-N17	174.42 (10)
Fe(B)-N16	2.003 (2)	N1-Fe(A)-N7	94.64 (9)	N20-Fe(B)-N19	81.02 (11)
Fe(B)-N17	1.908 (2)	N1-Fe(A)-N9	87.70 (9)	N20-Fe(B)-N21	79.77 (10)
Fe(B)-N18	2.001 (2)	N2-Fe(A)-N7	94.52 (8)	N14-Fe(C)-N15	77.19 (9)
Fe(B)-N19	1.981 (2)	N2-Fe(A)-N1	80.70 (9)	N14-Fe(C)-N10	121.04 (8)
Fe(B)-N20	1.889 (2)	N2-Fe(A)-N3	79.71 (9)	N14-Fe(C)-N12	88.09 (8)
Fe(B)-N21	1.974 (2)	N2-Fe(A)-N9	105.66 (8)	N14-Fe(C)-N13	72.79 (9)
Fe(C)-N10	2.149 (2)	N3-Fe(A)-N7	87.79 (9)	N15-Fe(C)-N10	101.77 (8)
Fe(C)-N11	2.115 (2)	N3-Fe(A)-N1	160.39 (8)	N15-Fe(C)-N12	91.47 (9)
Fe(C)-N12	2.268 (2)	N3-Fe(A)-N9	96.73 (8)	N15-Fe(C)-N13	149.83 (8)
Fe(C)-N13	2.298 (2)	N18-Fe(B)-N16	160.16 (10)	N11-Fe(C)-N14	150.64 (9)
Fe(C)-N14	2.122 (2)	N17-Fe(B)-N16	80.34 (10)	N11-Fe(C)-N15	124.20 (8)
Fe(C)-N15	2.146 (3)	N17-Fe(B)-N18	79.84 (11)	N11-Fe(C)-N10	77.38 (8)
		N17-Fe(B)-N19	98.54 (10)	N11-Fe(C)-N12	72.81 (8)
		N17-Fe(B)-N21	100.73 (9)	N11-Fe(C)-N13	85.01 (8)
		N19-Fe(B)-N16	86.94 (9)	N10-Fe(C)-N12	149.87 (8)
		N19-Fe(B)-N18	95.05 (9)	N10-Fe(C)-N13	91.23 (9)
				N12-Fe(C)-N13	90.50 (9)

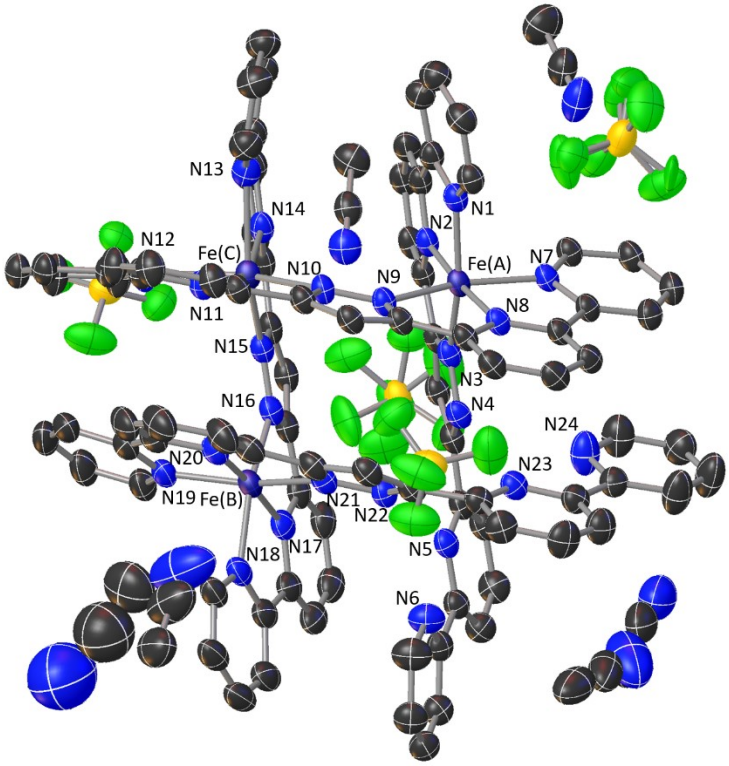

Figure S1. Asymmetric unit of the **FE3** grid at 100K. Hydrogen atoms are omitted for clarity.

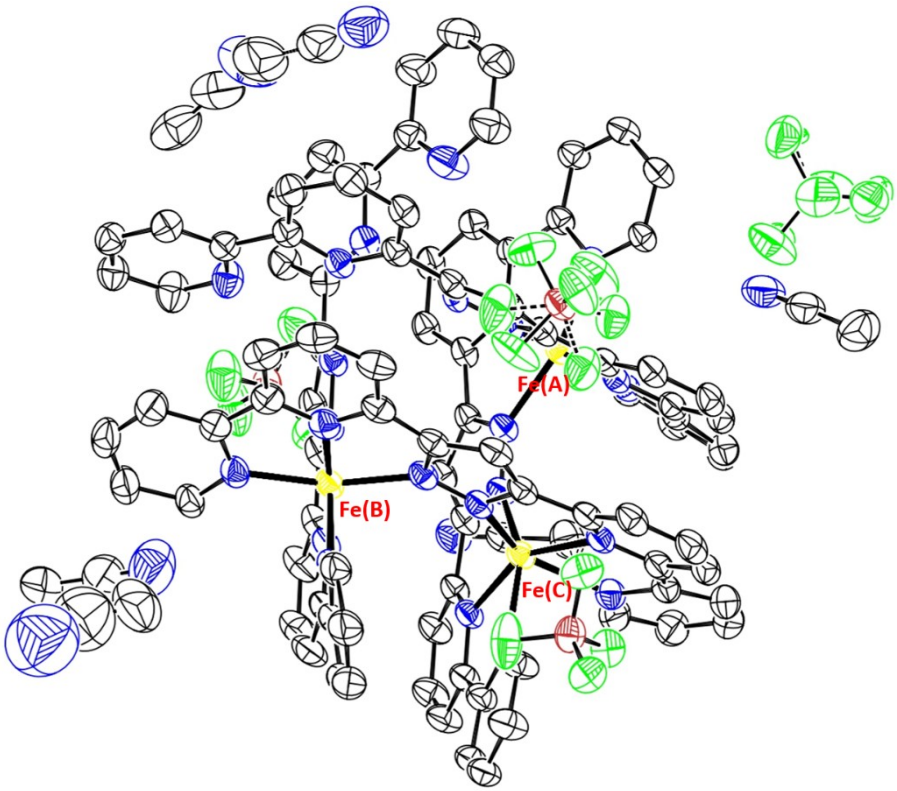

Figure S2. Thermal ellipsoid plot (50% of probability) for **FE3** at 100K. Hydrogen atoms are omitted for clarity.

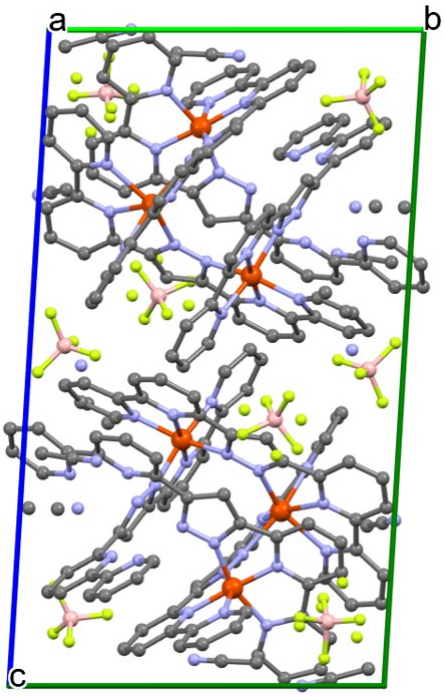

Figure S3. Packing of molecules down crystallographic '*a*' axis. Hydrogen atoms are omitted for clarity.

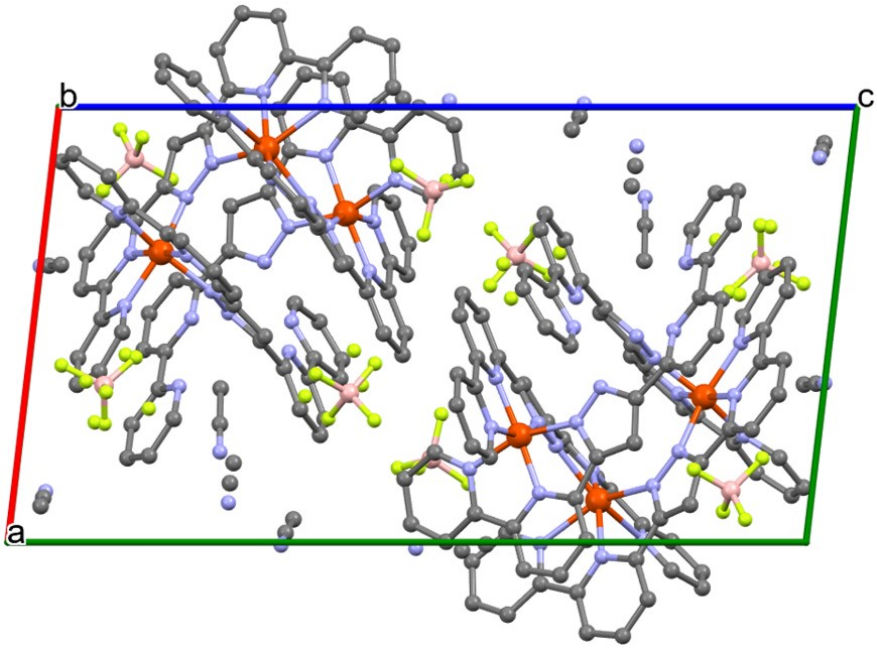

Figure S4. Packing of molecules down crystallographic '*b*' axis. Hydrogen atoms are omitted for clarity.

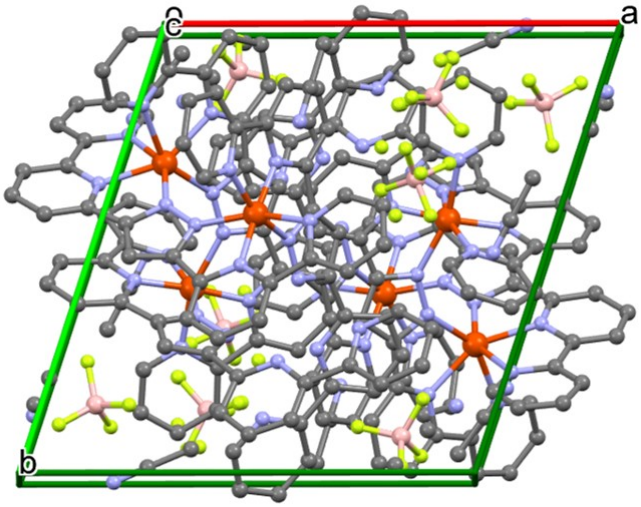

Figure S5. Packing of molecules down crystallographic '*c*' axis. Hydrogen atoms are omitted for clarity.

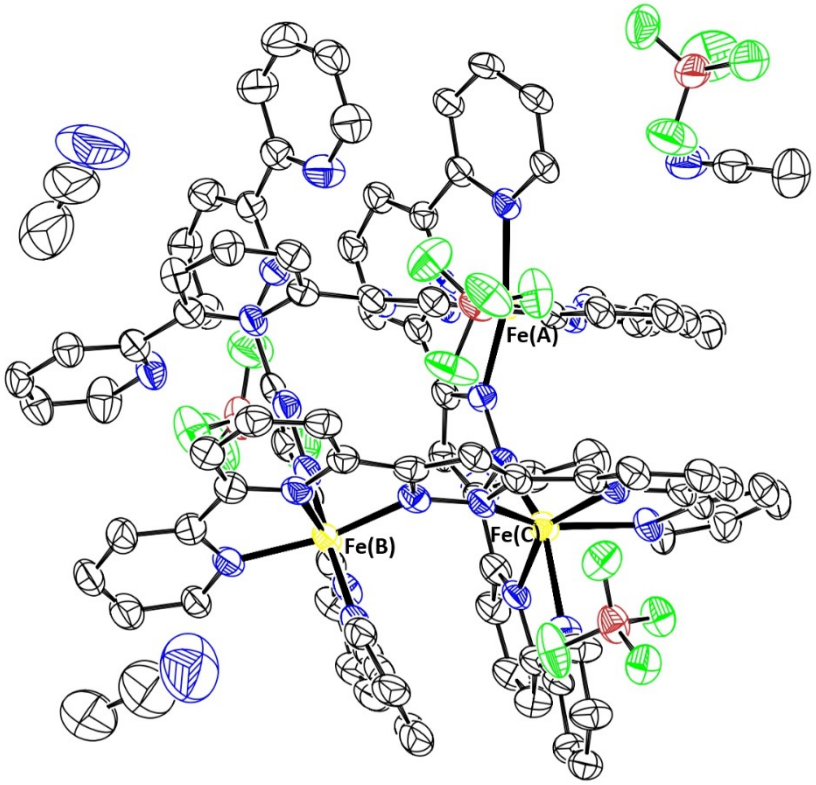

Figure S6. Thermal ellipsoid plot (50% of probability) for **FE3** for the -500ps data. Hydrogen atoms are omitted for clarity.

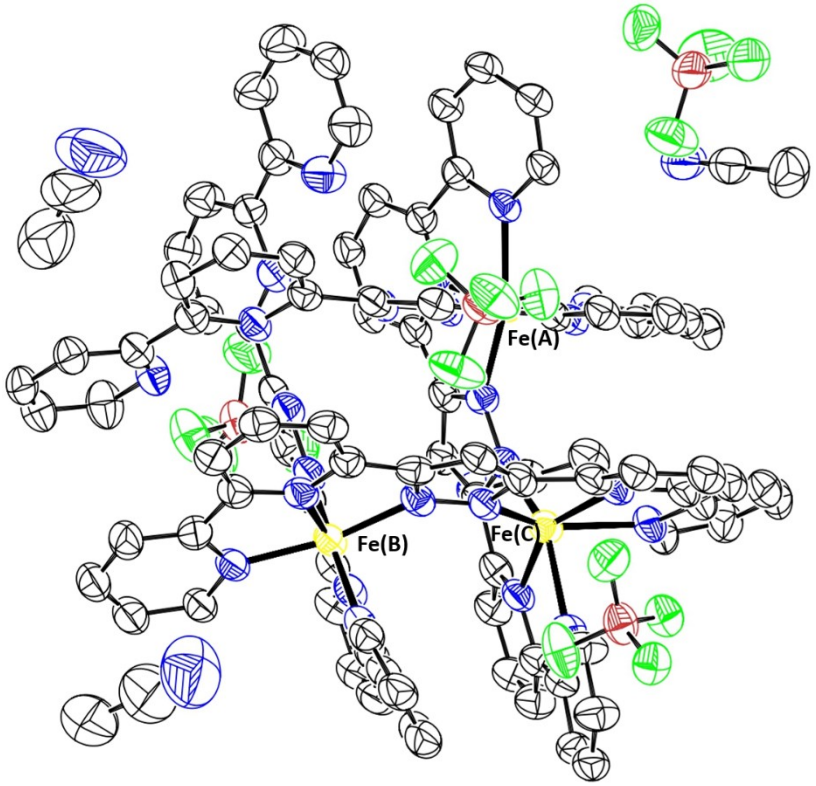

Figure S7. Thermal ellipsoid plot (50% of probability) for **FE3** for the 200pss data. Hydrogen atoms are omitted for clarity.

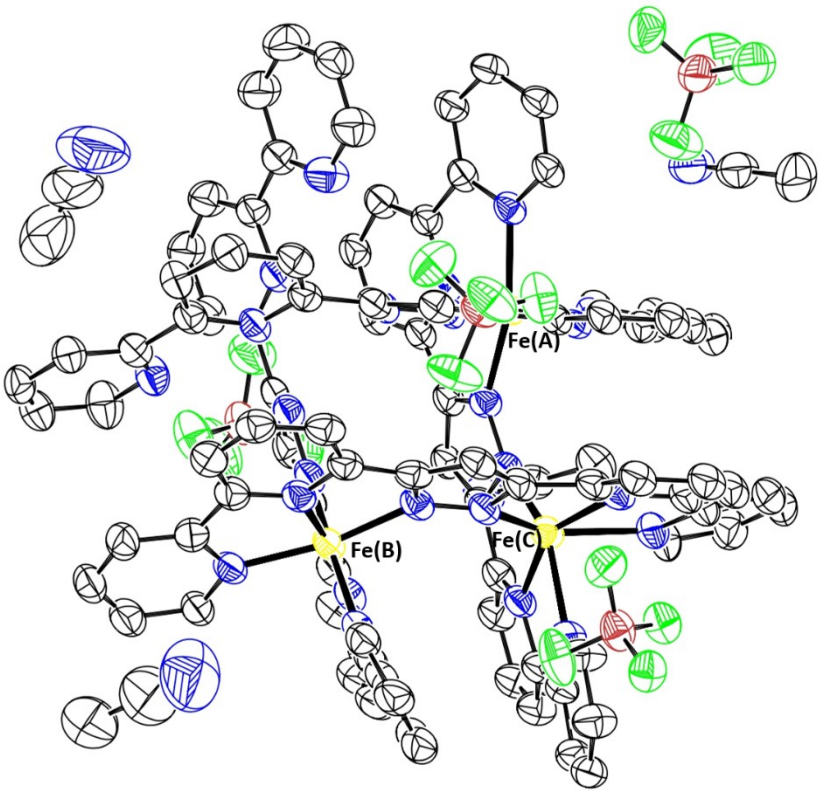

Figure S8. Thermal ellipsoid plot (50% of probability) for **FE3** for the 500ps data. Hydrogen atoms are omitted for clarity.

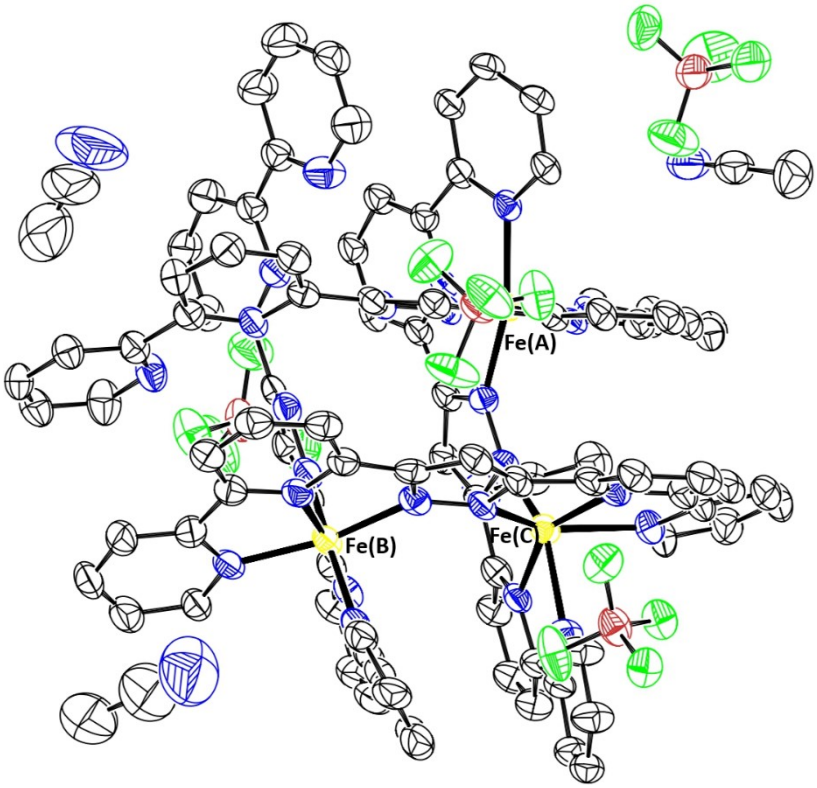

Figure S9. Thermal ellipsoid plot (50% of probability) for **FE3** for the 800ps data. Hydrogen atoms are omitted for clarity.

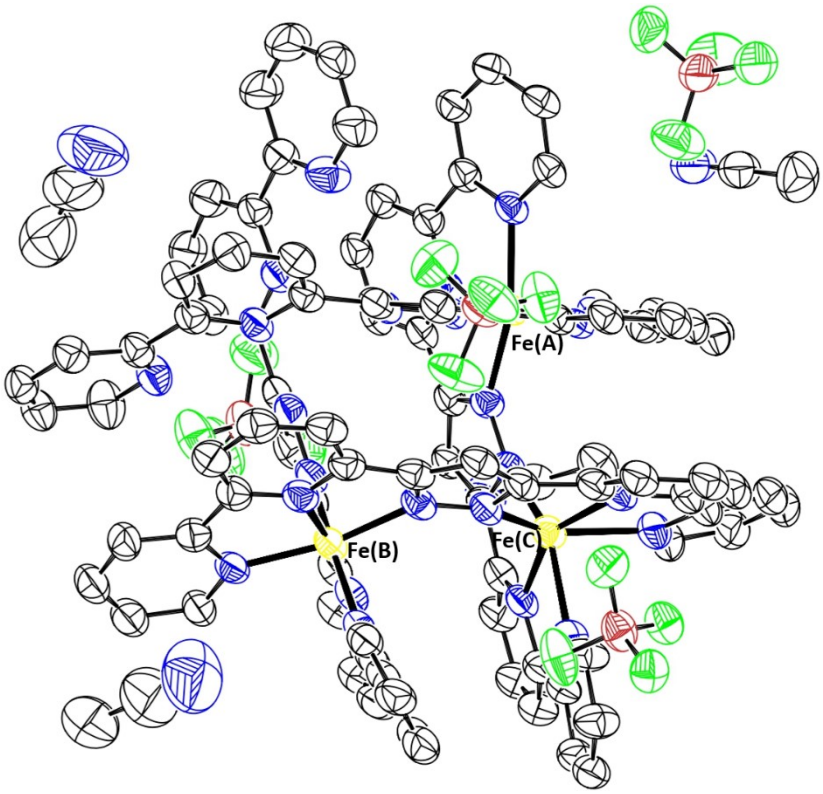

Figure S10. Thermal ellipsoid plot (50% of probability) for **FE3** for the 1ns data. Hydrogen atoms are omitted for clarity.

Structural Analysis

The Octadist program[1] was used to determine the <Fe-N> bond length and the angular distortion parameter that describes the octahedral coordination environment of the metal centres in the **FE3** grid. The angular distortion parameter, Θ, is the sum of the deviations from 60° of the 24 N-Fe-N angles, six per pseudo three-fold axis, measured on a projection of opposite triangular faces of the $\{FeN_6\}$ octahedron, orientated by superimposing the face centroids (Figure S1).[2,3]

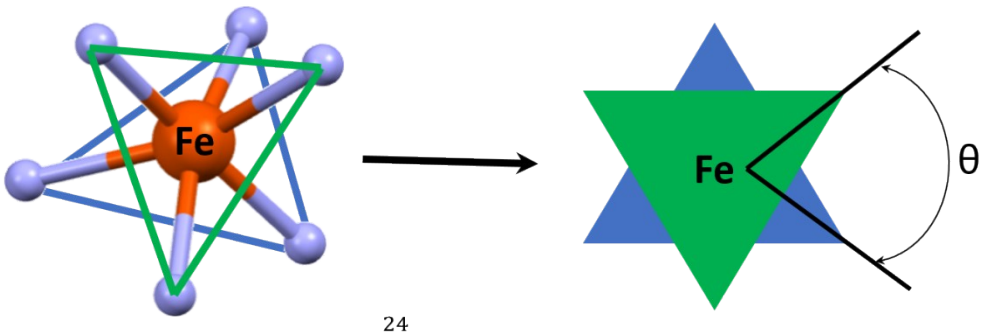

$$\Theta = \sum_{i=1}^{24} (\lfloor 60 - \theta_i \rfloor)$$

Figure S11. Environment of Fe^{II} ions and definition of the θ angle and the angular distortion parameter (Θ).[2,3]

For comparison, continuous shape measurements (CShM) were also used to characterise the relative deviation of the metal coordination spheres in **FE3** from ideal polyhedra described by a particular point symmetry group (Table S2).[4] Mathematically, CShM of the coordination polyhedron Q with the geometric centre $\vec{q}_0$ relative to an ideal polyhedron P is expressed as:

$$S_Q = min\left[\frac{\sum_{i=1}^{N} |\vec{q}_i - \vec{p}_i|^2}{\sum_{i=1}^{N} |\vec{q}_i - \vec{q}_0|^2}\right] \times 100 \qquad \text{(S1)}$$

where $\vec{q}_i$ and $\vec{p}_i$ are the position vectors for atoms of two polyhedra. CShM relative to an ideal octahedron (S(Oh)) and an ideal trigonal prism (S(itp)) were calculated using the SHAPE program.[5] The calculation of S(Oh) and S(itp) were performed for all crystallographic-symmetry independent metal atoms.

It is well known that the $\{FeN_6\}$ coordination sphere of LS Fe^{II} ions is more regular, i.e., closer to an ideal octahedron. Therefore, the S(Oh) parameter is small and closer to 0, while the parameter S(itp) >> 0. Contrarily, Fe^{II} ions in the HS state are characterised by a more irregular structure with structural parameters S(Oh) >> 0 and S(itp) closer to zero.

Estimate of Temperature Difference

A method for estimating the temperature difference between two different data sets collected at different temperatures is obtained from temperature-Wilson plots. The plots are obtained by a scale-factor refinement of the low temperature data (100K) with the high-temperature data (310K) structural model and plotting the $\ln(I^{100K}/I^{310K})$. The slope of the dependence of $\ln(I^{100K}/I^{310K})$ with $(\sin\theta/\lambda)^2$ gives the overall increase of isotropic atomic motion, ΔB (equation S2), which is associated with temperature difference between the data sets.[6]

$$ln\left(\frac{I^{100K}}{I^{310K}}\right) = -\,2\Delta B^{100K\,-\,310K}(sin\theta/\lambda)^2 \qquad \text{(S2)}$$

An analogous equation is used to calculate the temperature increase during the photo-crystallographic experiments. The energy deposited by the laser pulse largely exceeds the energy necessary for the LS to HS transition, which results in some heat diffusion and global warming. A modified Wilson plot, known as a photoWilson plot (Fig. S12), is then used to estimate the laser-induced temperature increase due to heat dissipation, in a similar way as described above for the temperature-Wilson plots. From the photoWilson plot, it is possible to calculate the variation of the isotropic temperature factor (ΔB)[6]:

$$ln\left(\frac{I^{dt}}{I^{dt<0}}\right) = -\,2\Delta B^{dt\,-\,dt<0}(sin\theta/\lambda)^2 \qquad \text{(S3)}$$

where I_{ON} and I_{OFF} are the laser-ON and laser-OFF intensities. Note that, in both cases, intensities must be brought to the same scale before calculating the value of ΔB.

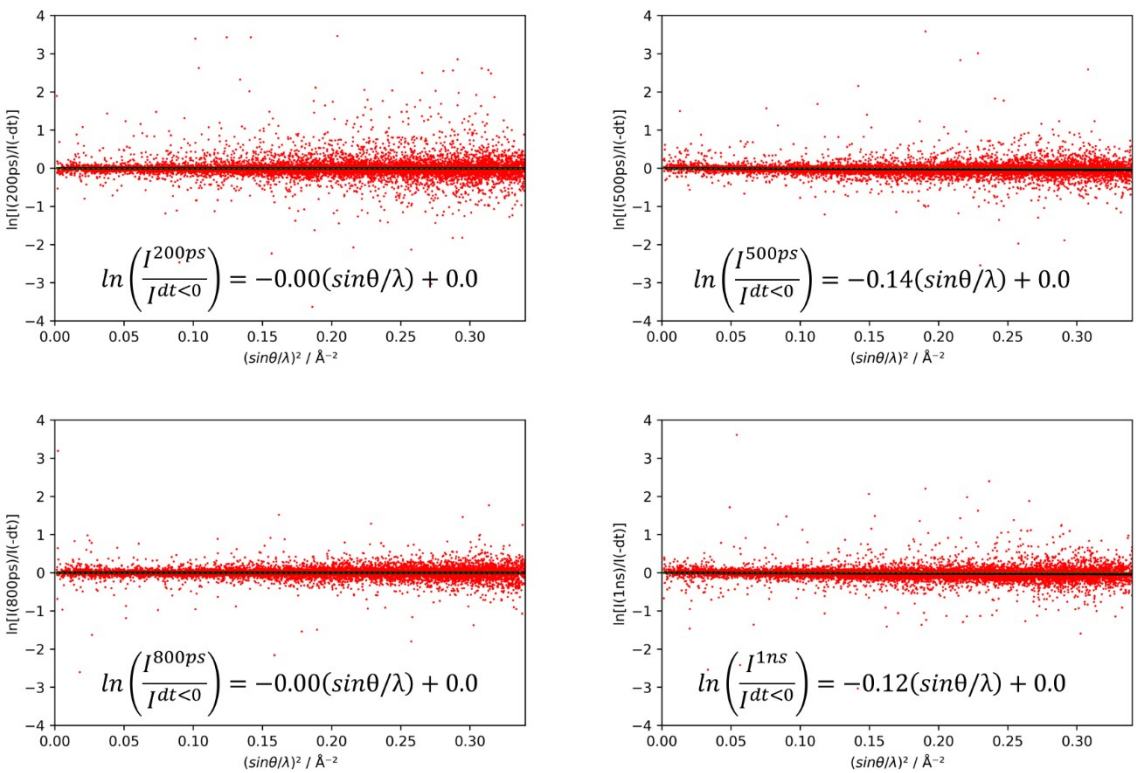

Figure S12. PhotoWilson plots of **FE3**.

Distortion

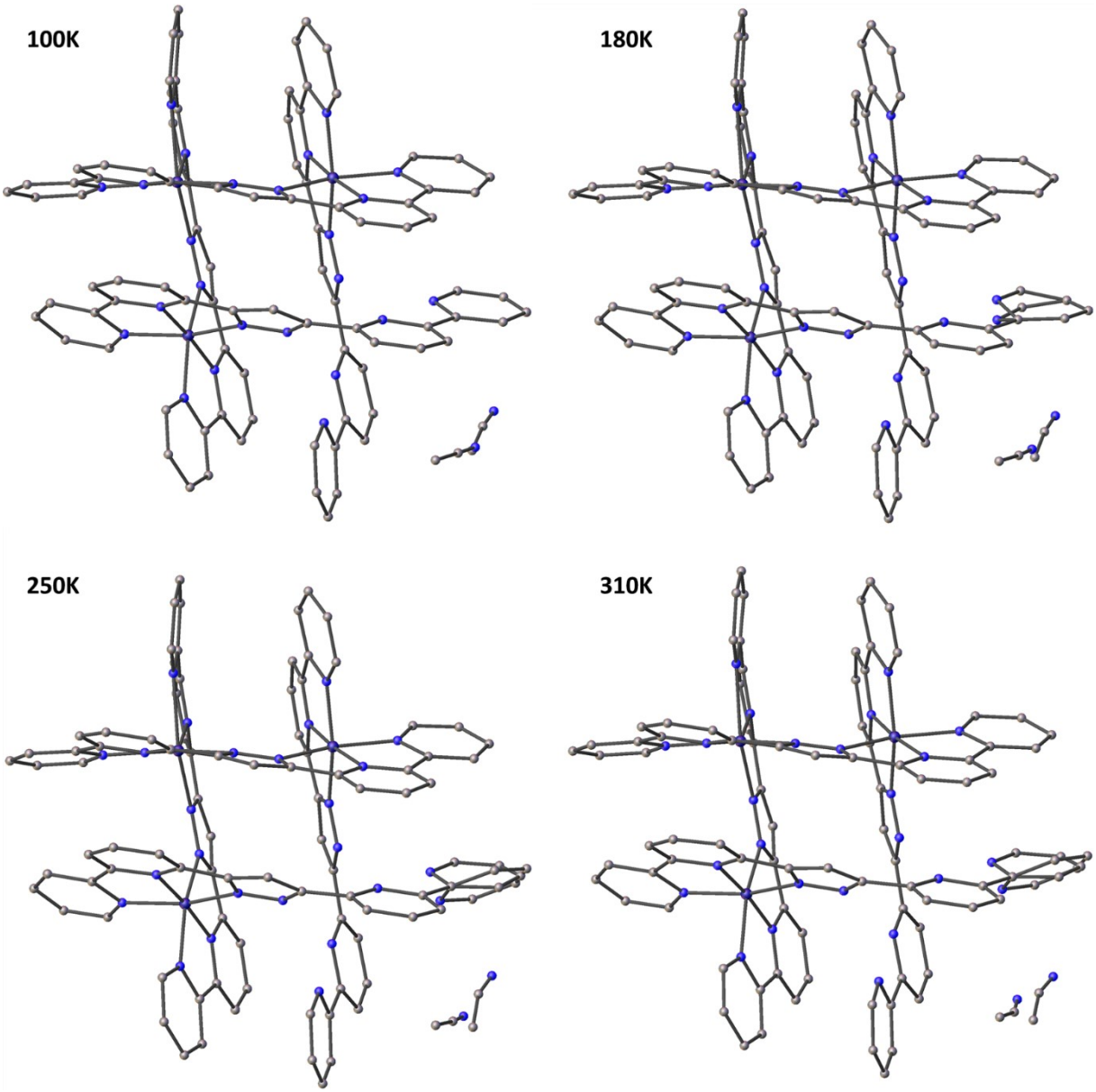

Figure S13. Molecular representation of the $[Fe_3L_4]^{4+}$ grid at different temperatures, showing the rotation of the pyridine ring and the nearest acetonitrile molecule refined as disordered over two positions.

Structural Details

Table S3. Structural data that provides a basic description of the SCO in **FE3**.

Structural parameter	100K	250K	310K
		Fe(A)	
<Fe-N> (Å)	1.966 (2)	1.968 (2)	1.974 (2)
S(Oh)	2.256	2.290	2.332
S(itp)	11.159	11.060	10.968
Σ (°)	95.44	93.89	95.12
Θ (°)	306.06	310.54	313.53
ζ (Å)	0.234	0.232	0.231
Vp (Å^3)	9.771	9.797	9.877
		Fe(B)	
<Fe-N> (Å)	1.959 (2)	1.964 (2)	1.968 (3)
S(Oh)	2.183	2.198	2.284
S(itp)	11.201	11.027	10.904
Σ (°)	94.70	92.75	93.71
Θ (°)	301.94	302.60	310.47
ζ (Å)	0.243	0.242	0.220
Vp (Å^3)	9.687	9.750	9.802
		Fe(C)	
<Fe-N> (Å)	2.183 (2)	2.187 (2)	2.188 (3)
S(Oh)	6.140	6.156	6.160
S(itp)	6.475	6.572	6.495
Σ (°)	146.93	146.36	145.31
Θ (°)	577.25	576.38	575.71
ζ (Å)	0.401	0.396	0.394
Vp (Å^3)	12.285	12.356	12.388
		Molecular Scale	
Superposition of structures	100K (blue) & 250 K (red)		100K (blue) & 310 K (red)
	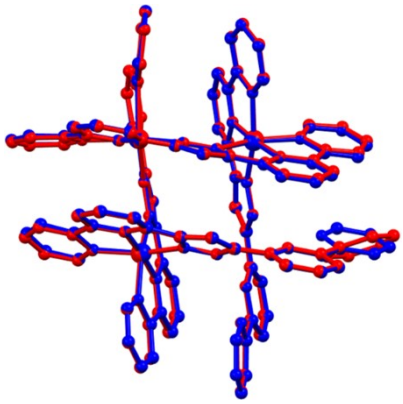		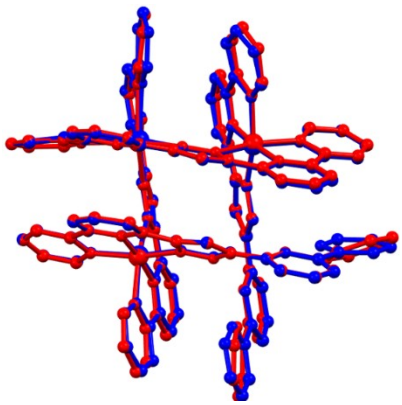
Maximum RMSD	1.1862		0.8101
Average RMSD	0.1925		0.1965
		Unit cell Changes	
a (Å)	14.010 (3)	14.150 (3)	14.240 (3)
b (Å)	14.480 (3)	14.590 (3)	14.630 (3)
c (Å)	24.320 (5)	24.710 (5)	24.860 (5)
V (Å^3)	4667.1 (18)	4797.6 (19)	4863.8 (19)
		Crystal packing	

Intermolecular interactions (Å)	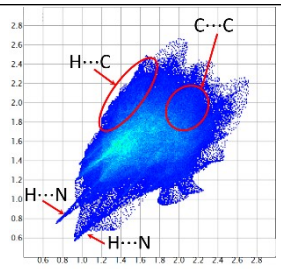	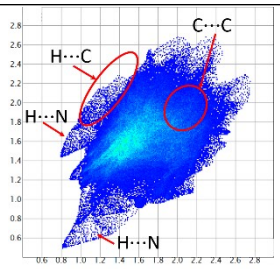	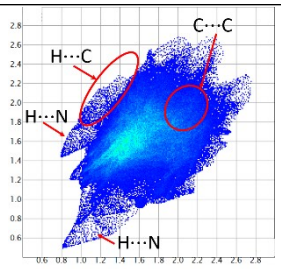
Separation between π-π planes (Å)	4.224, 4.837	4.356, 5.014	4.425, 5.076
Crystal density	1.553	1.511	1.484

$\Sigma=\Sigma^{12}_{i=1}|90 - \phi_i|$, the sum of the angular deviations from 90° for the 12 cis angles (ϕ_i)[7,8], $\Theta = \Sigma^{24}_{i=1}|60 - \theta_i|^2$, $\zeta=(Fe\text{-}N_i) - \langle Fe\text{-}N\rangle$[9]. Information about Θ, S(Oh) and S(itp) is provided in the structural analysis section.

References

1 R. Ketkaew, Y. Tantirungrotechai, P. Harding, G. Chastanet, P. Guionneau, M. Marchivie and D. J. Harding, *Dalton Trans*, 2021, **50**, 1086–1096.

2 M. Marchivie, P. Guionneau, J.-F. Létard and D. Chasseau, *Acta Crystallogr. B*, 2005, **61**, 25–28.

3 M. Marchivie, P. Guionneau, J.-F. Létard and D. Chasseau, *Acta Crystallogr. B*, 2003, **59**, 479–486.

4 H. Zabrodsky, S. Peleg and D. Avnir, *J. Am. Chem. Soc.*, 1992, **114**, 7843–7851.

5 M. Llunell, D. Casanova, J. Cirera, P. Alemany and S. Alvarez, *SHAPE program, version 2.1*, Barcelona, 2003.

6 M. S. Schmøkel, R. Kamiński, J. B. Benedict and P. Coppens, *Acta Crystallogr. A*, 2010, **66**, 632–636.

7 P. Guionneau, M. Marchivie, G. Bravic, J.-F. Létard and D. Chasseau, in *Spin Crossover in Transition Metal Compounds II*, eds. P. Gütlich and H. A. Goodwin, Springer Berlin Heidelberg, Berlin, Heidelberg, 2004, pp. 97–128.

8 M. A. Halcrow, *Chem. Soc. Rev.*, 2011, **40**, 4119.

9 M. Buron-Le Cointe, J. Hébert, C. Baldé, N. Moisan, L. Toupet, P. Guionneau, J. F. Létard, E. Freysz, H. Cailleau and E. Collet, *Phys. Rev. B*, , DOI:10.1103/PhysRevB.85.064114.